Journal of Materials Chemistry B

PAPER

View Article Online
View Journal | View Issue

Cite this: J. Mater. Chem. B, 2016, 4, 2153

Study on the bio-functionalization of memristive nanowires for optimum memristive biosensors

I. Tzouvadaki,*[a] N. Madaboosi,[b] I. Taurino,[a] V. Chu,[b] J. P. Conde,[bc] G. De Micheli[a] and S. Carrara[a]

Received 25th January 2016,
Accepted 16th February 2016

DOI: 10.1039/c6tb00222f

www.rsc.org/MaterialsB

Semiconductor nanowires are emerging as promising building blocks for biosensors enabling direct electrical detection of various biomolecules. In this framework, two-terminal Schottky-barrier silicon (Si) nanowire arrays that exhibit memristive electrical response, so-called memristive devices, are bio-functionalized and converted to memristive biosensors for bio-detection purposes. A comparative analysis of three bio-functionalization strategies is proposed here in order to design and develop optimum memristive biosensors to be implemented in label-free sensing applications. The surface of the device is modified with an anti-free-Prostate Specific Antigen (PSA) antibody as the case of study *via*: (a) direct adsorption on the device surface, (b) a bio-affinity approach using biotin–streptavidin combination and (c) covalent attachment using (3-glycidyloxypropyl)trimethoxysilane (GPTES). The optimum memristive biosensor is defined *via* the calibration and comparative study of the biosensors' electrical response under controlled environmental conditions (humidity and temperature) in order to maximize the performance of the biosensor. In addition, it is demonstrated that the direct passive adsorption strategy presents double the performance of the other two methods. The uptake of biological molecules on the nanostructure surface is verified by atomic force microscopy and confocal microscopy. Scanning electron microscopy reveals the details of the surface morphology of the nanofabricated structures before and after bio-functionalization for the three methods applied. The system shows potential for general application in molecular diagnostics, and, in particular, for the early detection of prostate cancer.

Introduction

As the demand for new biosensors for early disease diagnosis and prognosis has increased over recent years, the research into developing a new biosensor design, including the development of new biomolecular immobilization technologies, has drawn considerable attention.[1] Label-free assays have been successfully applied in biochemical screening applications, which involve protein–protein, protein–DNA, protein–peptide and protein–small-molecule interactions. The ability to characterize binding pairs without developing reagents or labels is a great advantage as it reduces the resources required for assay development and time, simplifies the assay design and minimizes drawbacks created by the use of labels such as photobleaching and the need for optical filters. Furthermore, labeling can, in some cases, either block the active site of target proteins or lead to significant changes in the conformation of the protein that affect its function. Label-free assays can potentially overcome these deficiencies providing both sensitivity and specificity, qualities that depend on both the device performance itself and the surface functionalization method as well.[2–4]

Reducing cost and time is one major concern in clinical diagnostics, particularly in molecular diagnostics. Miniaturization technologies have been recognized as promising solutions to provide low-cost microchips for diagnostics. The lower volumes of reagents and molecules required for miniaturized technologies can significantly reduce the total cost and waste. Furthermore, miniaturized bioassays can be integrated with microelectronics and microfluidics for the development of a fully automated system allowing rapid molecular analysis.[5] Semiconductor nanowires and semiconducting carbon nanotubes are frequently reported for their applications as components of miniaturized bio-assays and their potential in the label-free detection of diverse biomolecules. Nanowire structures present a high surface-to-volume ratio and consequently their electrical properties are strongly influenced by even minor perturbations.[6,7] Furthermore, the nanowire structures exhibit tunable electron transport properties and the charge accumulation or depletion takes place in the bulk of the structure. These properties lead to a

[a] Integrated System Laboratory EPFL, Lausanne, Switzerland. E-mail: ioulia.tzouvadaki@epfl.ch; Fax: +41 216930909; Tel: +41 216934243
[b] INESC Microsistemas e Nanotecnologias and IN-Institute of Nanoscience and Nanotechnology, Rua Alves Redol, 9, Lisbon 1000-029, Portugal
[c] Department of Bioengineering, Instituto Superior Técnico, University of Lisbon, Av. Rovisco Pais, 1, Lisbon 1049-001, Portugal

highly sensitive electrical response. First, the device surface is accordingly treated to allow only the binding of the target molecules for bio-detection, thus preventing non-specific binding. Then, the conductance of these devices changes when a target molecule binds to the surface of the device. This 'electrochemical gating' arises from a change in local surface potential induced by target binding or other changes like the solution pH in the immediate vicinity of the nanowire.[8]

Consequently, these nanostructures may enable label-free sensing *via* direct electrical readout when the nanostructures are used as semiconducting channels of field-effect transistors,[9] for example for cancer markers[10] or DNA detection.[11] Moreover, Si nanowire field-effect transistors (FETs) can be used as biosensors to measure protein–ligand binding affinities and kinetics with sensitivities down to femtomolar concentrations.[12] In addition, Si nanowire FETs can directly translate the analyte–surface interaction into an electrical signal, providing real-time ultrasensitive high throughput detection of the desired biomolecules, without the requirement for any labels.[13]

Memory effects appear frequently in nature, for example, the information gathered, stored and retrieved in synaptic connections in the brain,[14] mechanical information stored in the spatial configuration of polymer side-chains,[15] and memory effects existing in molecular organization.[16] Pronounced hysteresis in electrical characteristics is a unique and important signature of memory effects in electronic-based devices.[17] These electrical hysteresis effects have been attributed to a wide range of possible phenomena, including molecular redox events and metal filament formation and destruction. The theory for a broad range of systems showing this memory effect was developed initially by Chua and Kang[18,19] and more recently by Strukov *et al.*[20] These memristive systems are passive systems that fall under the domain of non-linear circuit theory and possess memory capability as they can maintain their specific state in the absence of an applied bias. This effect is observed at the nano-scale level where the current *versus* voltage characteristics appear as hysteresis loops. Several different nanofabricated devices, such as memcapacitors and meminductors, manifest memory effects similar to those described by Chua and Kang.[18,19] In all these structures, the memory effect depends on the rearrangement of charge carriers at the nanoscale due to external perturbations.[21] These memory-effect devices have been fabricated using different materials, including Poly-Si,[22] crystalline Si,[23] platinum/TiO_2,[24] aniline-derivatized conductive-polymers,[25] and graphene embedded in insulating polymers.[26] Furthermore, memristive devices have been proposed for implementation in a wide variety of applications including digital[24] and analog[27] memory devices, and logic[28] and neuromorphic[29] circuits. Memristive devices enable new possibilities for computation and non-volatile memory storage, such as, for example, the construction of memristor-based digital logic circuits,[30] applications regarding artificial synapses,[31–33] Resistive RAMs (ReRAMs)[34] and Generic Memristive Structure (GMS) for 3-D Field Programmable Gate Array (FPGA) applications.[35]

Moreover, two-terminal Schottky barrier Si nanowire devices exhibiting memristive electrical response are implemented for bio-detection purposes leveraging the hysteresis modification after bio-functionalization with antibodies and the masking contribution to this effect introduced by the antigen uptake.[36,37]

Thus, an optimum memristive biosensor is expected to provide, initially, a large voltage gap. An adequately large voltage gap after bio-functionalization enables efficient antigen sensing offering the possibility to detect and discriminate antigen concentrations over a wide range and can potentially increase the performance of the memristive biosensor. The present work presents a comparative analysis of three bio-functionalization strategies using an anti-free-PSA antibody as the case of study, under varying environmental conditions, for the fabrication of optimum, high performance nanofabricated memristive biosensors.

Materials and methods

Fabrication of memristive biosensors

Memristive Si nanowire Devices are fabricated through a top-down fabrication process as previously described in ref. 38. Memristive biosensors are fabricated *via* surface bio-modification of memristive devices. First, the devices are incubated in a fresh Piranha solution ($H_2O_2 : H_2SO_4$ in a ratio of 3 : 1) for 25 min in order to remove any organic residues from the sample surfaces as well as to generate more free surface hydroxyl-terminating groups, making the surface highly hydrophilic. Hydroxyl groups serve as surface treatment, enabling a stable chemical attachment of the biomolecules. Subsequently, substrates of Si nanowire arrays fabricated in the same processing run are separately bio-functionalized following three different bio-modification approaches that are illustrated through the schematic presented in Fig. 1: (a) direct passive adsorption on the device surface; (b) a bio-affinity approach using a biotin–streptavidin combination; and (c) covalent attachment using GPTES. The antibody solution consists of an anti-free-PSA antibody diluted in filtered Phosphate Buffered Saline (PBS) solution (from here onwards, use of PBS refers to a PBS solution of pH 7.4 filtered through a syringe filter with a 0.4 μm pore size. In addition this solution is used for all dilution and rinsing steps in the present study, unless otherwise mentioned). After each incubation, all the substrates are gently washed three times for 5 min with PBS, and then are gently though completely dried with gentle nitrogen (N_2) flow before the measurements. All the measurements are performed immediately after every bio-functionalization process is completed.

Method A: passive adsorption. The nanostructures are incubated overnight at RT in a 250 μg mL^{-1} Anti-PSA antibody (Abcam – ab10185) in PBS. The antibody solution is deposited on the surface of the substrate by standard drop casting using a micropipette directly on the area of interest. After incubation, the substrate is gently washed and dried as previously described.

Method B: affinity approach. In parallel, nanowire structures are separately incubated for 4 h at RT, in 200 μg mL^{-1} biotin (biotin ≥ 99% (TLC), lyophilized powder (Sigma-Aldrich – B4501); a concentration of 1 mg mL^{-1} in MilliQ water, in PBS).

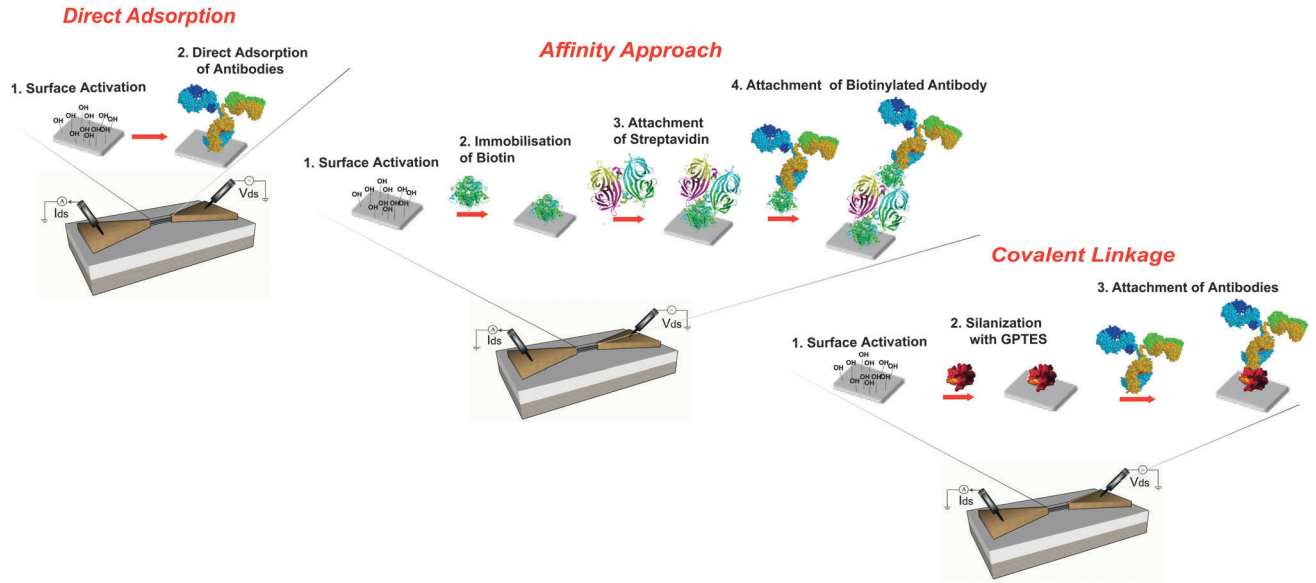

Fig. 1 Graphical abstract illustrating the experimental platform. Memristive nanowire devices anchored between two pads serving for the electrical characterization are bio-functionalized following three bio-functionalization strategies.

After rinsing the surface thrice with PBS, a further 4 h incubation follows in 100 μg mL^{-1} streptavidin (streptavidin from *Streptomyces avidinii* (Sigma-Aldrich – S4762); a concentration of 1 mg mL^{-1} in MilliQ water, in PBS). The substrates modified with the biotin–streptavidin complex are subjected to an overnight incubation at RT in 250 μg mL^{-1} solution of a biotinylated anti-PSA antibody (Abcam – ab182031) in PBS. After incubation, the so-obtained devices are gently washed and dried with N_2 flow.

Method C: covalent attachment. In addition, nanowire devices are separately functionalized by exposing the surface to GPTES solution (1% in ethanol containing 10 mM acetic acid) for 1.5 h at RT. What follows is extensive rinsing in ethanol with 10 mM acetic acid to remove unreacted GPTES. Antibody attachment is carried out by exposing the surface to antibodies through overnight incubation in 250 μg mL^{-1} anti-PSA antibody (Abcam – ab10185) at RT. The devices are then washed with PBS and completely dried with N_2 flow as previously mentioned.

Electrical characterization

The electrical characteristics of the nanofabricated memristive structures with an initial mean width of 38 nm and a length of 410 nm are obtained by measuring the current–voltage characteristics of the devices in air on dried samples using a Cascade Microtech Probe Station and a Hewlett–Packard 4165A Precision Semiconductor Parameter Analyzer. The current flowing through the two terminals of the nanowire channel is acquired as the source to drain current *versus* the potential applied to these terminals. For the sensing measurement, a drain to source voltage double sweep is performed, forward and backward, in the range of −2.4 V to +2.4 V. The back-gate potential V_{BG} is kept grounded during the acquisition. All the measurements are carried out at RT in a controlled humidity environment as mentioned before. A reference measurement is first made on the nanostructures just after the fabrication process, followed by the electrical monitoring of the bio-modified memristive nanostructures for the bio-functionalization approaches under study. A statistical analysis is performed on a sufficiently large number of devices and the average value of the voltage gap is presented with respect to the rH% windows.

The temperature and the relative humidity (rH%) monitoring is performed using feedback from a Rotronic HC2-C04 Thermo-Hygrometer tool, while varying the environmental humidity in the measurement chamber. The Rotronic HW4 tool provides an accurate control of the relative humidity and temperature of the measurement environment. All measurements are acquired at RT. A wet towel is introduced into the measurement chamber in order to increase the humidity, while the sodium chloride ACS reagent, ≥99.0% (Sigma-Aldrich – S9888), is used to achieve lower humidity values. Before the measurement procedure, a waiting time of 2 h is necessary in order to establish stable environmental conditions in the measuring chamber. In addition, before each individual measurement, a waiting time of 5 min to 20 min is necessary for regaining the equilibrium of the environmental conditions. Unstable humidity and temperature conditions during the measurements result in the introduction of significant noise to the electrical characteristics of the sensing devices, altering the electrical readout, and may ultimately inhibit the bio-detection mechanism. The control of the humidity during the acquisition is not straightforward. Because of that, the acquisition of the curve from the same memristive devices, before and after the functionalization, could not be performed at exactly the same rH% values, but similar humidity windows were taken into account.

Surface and morphological characterization

Morphological Atomic Force Microscopy (AFM) analysis of the nanofabricated structures of width 38 nm and a length of

410 nm is performed using a Bruker Atomic Force Microscope system. The AFM measurements are carried out on bare samples directly after the fabrication process and after the bio-modification of the surface with an anti-PSA antibody. In order to obtain accurate morphological information for the nanofabricated devices prior to and after bio-modification, imaging is carried out using the PeakForce Tapping mechanism, which decouples cantilever response from resonance dynamics, to automatically adjust all critical imaging parameters. Direct interaction force control enables the production of a uniformly optimized feedback loop for all the points of the sample. The resulting force-curves are extracted, correlated with the sample topography, and analyzed using the NanoScope analysis software. Furthermore, confocal microscopy (CLSM) is performed using a ZEISS LSM 710 for obtaining a 3D fluorescent signal distribution of the biomolecules. For this purpose, a substrate of Si nanowire arrays of width 150 nm and a length of 4.8 μm originating from the same fabrication run is separately incubated overnight at RT and in the dark, in 50 μg mL^{-1} of anti-mouse IgG-FITC (Sigma – F9006) in PBS, gently washed three times with PBS and dried with N_2 flow. In parallel, a negative control sample consisting of unmodified nanostructures is imaged. In addition, a Scanning Electron Microscopy (SEM) analysis of the nanofabricated structures of mean width 90 nm and length 980 nm is carried out using the Scanning Electron Microscope Gemini500 from Zeiss, directly after the nanofabrication process and also after bio-functionalization. A 2 nm layer of iridium (Ir) is sputtered onto the bio-functionalized devices in order to avoid the protein charging effect and to provide the needed contrast to images.

Results and discussion

Analytical performance

The electrical characterization performed on bare nanofabricated wires indicates a hysteretic loop at zero voltage for the forward and the backward curves of the current, as depicted in Fig. 2a. In these devices, the memory effect depends on the charge carrier rearrangement at the nanoscale due to external perturbations, like for example an applied bias. Nevertheless, when biological substances are present on the device surface, the hysteresis shifts from that observed at zero voltage and the current minima for the forward and the backward regimes occur at different voltage values as shown in Fig. 2b. In this case, a voltage gap is created in the semi-logarithmic current–voltage characteristics after the nanowire bio-modification as a further memory effect on the voltage scan across the memristive nanostructure. The presence of biological substances around the freestanding nanowire contributes to extra charges surrounding the device creating an electrical field surrounding the channel of the memristive device, resulting in an all-around bio-gate effect equivalent to that exhibited by nanostructures without any bio-functionalization but fabricated using an all-around Si gate that controls the channel current.[37] Thus, the attachment of biomolecules on the nanostructure produces a conductance change that affects the electrical response of the nanodevice, as clearly shown by the graphs. The two main factors that affect the memristive signals and the biosensor performance, the relative humidity (rH%) due to the environmental conditions and the bio-functionalization strategy applied, are studied.

relative Humidity (rH%). The effect of varying environmental humidity conditions on the electrical response of the nanodevice is studied and presented in Fig. 3 initially for bare nanostructures directly after the fabrication process and then for the same nanostructures bio-modified *via* the bio-functionalization strategies under study, in the same rH% window. Each voltage gap point represents the mean value of the voltage gap values obtained by the electrical characterization of a set of single devices.

The average voltage gap value exhibited by bare nanostructures just after the fabrication process is shown in Fig. 3. Five individual substrates consisting of nanowire structures, originating from the

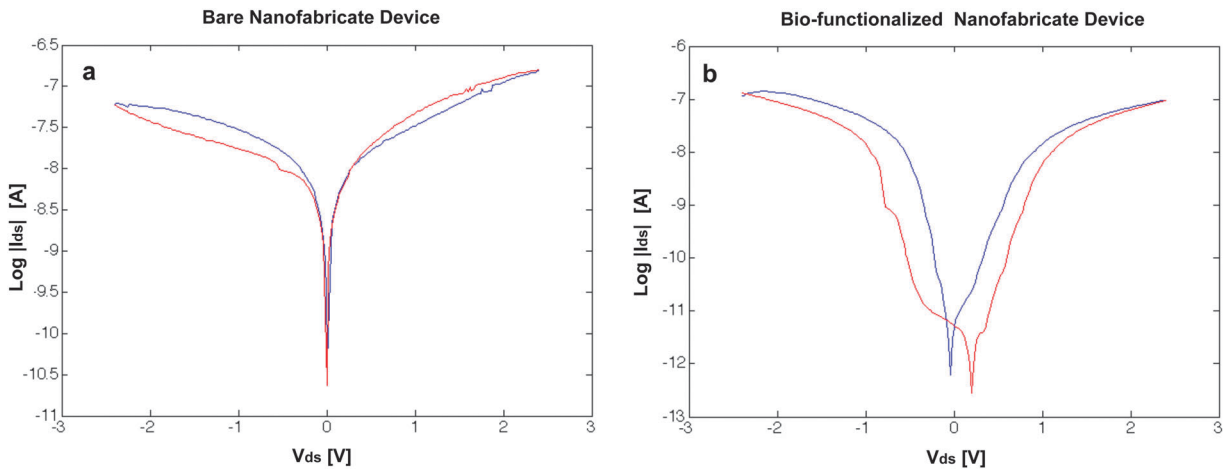

Fig. 2 Semi-logarithmic current to voltage characteristics demonstrating the memristive behavior of a bare nanofabricated device (a) and of a bio-functionalized device using an anti-PSA antibody (b), presenting a voltage gap of 0.24 V. Colors indicate forward (red) and backward (blue) regimes respectively.

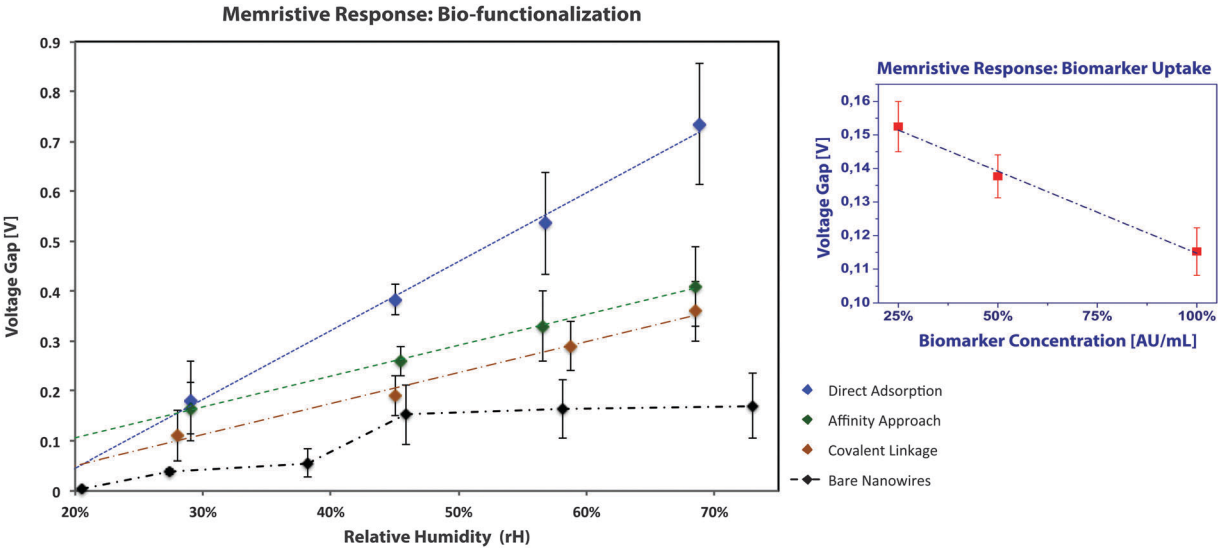

Fig. 3 Average voltage gap values exhibited by non-bio modified nanostructures just after the fabrication process tested under different relative humidity conditions (rH%) and after the implementation of three different bio-functionalization methodologies at the same relative humidity windows. The reported error bars describe the standard deviation of the voltage gap measured for all the devices under study indicatively for each case of bio-functionalization strategy and for each rH% regime. This error is also highly dependent on the top-down fabrication process, which cannot result in perfectly homogenous structures and to non-homogeneous distribution of biological species in functionalized nanowires, a fact that is also confirmed by SEM imaging. In the inset figure, the voltage gap response is presented with respect to the concentration of antigen uptake. The results are obtained at rH 25% for the binding pair Polyclonal Rabbit anti-human PSA – PSA-IgM.

same fabrication process and the same SOI wafer are electrically characterized focusing on a set of eighteen nanowire devices for each substrate at six rH% windows, in order to obtain significant statistical measurements of the electrical behavior. It is observed that for low rH%, the voltage gap value for bare devices is zero or close to zero values. By increasing the rH%, a small voltage difference appears between the forward and the backward regimes, due to the presence of water molecules originating from the environmental humidity that adsorb and accumulate on the nanowire surface. Those molecules finally form a thin liquid film on the nanowire surface. The voltage gap value increases with respect to the humidity but remains below the gap that develops upon bio-functionalization. In addition, after 45% of rH%, the voltage gap is almost constant and the system appears to be saturated. The voltage gap values in the case of bare devices are in the range of 0–0.16 V and demonstrate the stability of the device prior to any modification with respect to the humid environment.

The average voltage gap value exhibited by the above described nanostructures after surface treatment with biomolecules is also presented in Fig. 3 for the three bio-functionalization strategies. The results are obtained by the electrical characterization of a set of sixteen devices for each bio-functionalization strategy in the same rH% windows. Unlike bare devices exhibiting small voltage gap values, bio-functionalized nanostructures characterized under the same rH% windows show greater differences at the positions of the current minima for backward and forward regimes. An increasing trend of the voltage gap with respect to the rH% value is depicted for the bio-modified devices for all the bio-functionalization methods applied. By increasing the rH%, the voltage difference appearing between the forward and the backward regimes significantly increases due to the absorption of water molecules by hydrophilic biological substances, and in this case it is significantly larger than the absorption of water molecules occurring at the surface of a non-bio-modified nanodevice.

Any protein consists of hydrophobic and hydrophilic charged residues, and antibodies under physiological conditions presents positively charged residues in excess.[37] However, proteins isolated under totally dry conditions are considered poor conductors[39,40] and the basic reason for this is that the valence and conduction levels of extended electronic states of protein structures are separated by such a wide energy gap that at RT there is a negligible probability for the intrinsic generation of mobile charge carriers. Taking into consideration the existence of mobile charges, whose short- and long-range hopping motion strongly depends on the physical state of the protein-bound water, one of the main effects of increasing protein hydration is to increase the effective mobility of the dominant charge carriers.[41] Overall, the presence of a thin water molecule layer on the nanodevice surface activates the charge conductance and the increase of the humidity further enhances this mechanism.

Bio-functionalization strategy. Considering the comparative analysis of the three bio-functionalization techniques under study, the results obtained by electrical characterization shown in Fig. 3 depict that all three strategies applied lead to the development of a voltage gap after the bio-functionalization step. Therefore, it can be concluded that all bio-functionalization methods studied present the potential for further applications through the memristive bio-detection method and the voltage gap modification in future applications for PSA sensing, a Prostate

Cancer biomarker. Nevertheless, since the focus of the present study is to optimize the memristive biosensor, the environmental condition levels play a pivotal role when deciding which is the most suitable bio-functionalization technique.

It is observed that for low rH%, the three different methods result in similar voltage gaps, with the affinity methodology showing slightly higher gaps than the other two methods. However, by increasing the environmental humidity, the direct adsorption methodology becomes increasingly more effective compared to affinity and covalent attachment strategies. Both biotin, a thiol organosulfur compound, and GPTES are small hydrophobic molecules; therefore there is not a considerable positive contribution towards the water absorption mechanism. Regarding the presence of protein residues on the nanodevice surface, antibodies possess more functional groups that interact with water molecules compared to streptavidin. More specifically, the antibodies are longer structures containing more amino acids that are hydrophilic compared to streptavidin. Taking into consideration the fragment crystallizable region (Fc region) and fragment antigen-binding (Fab fragment) of an IgG antibody, the antibody structure is more hydrophilic than streptavidin, according to the Hopp–Woods plots for the ranking of amino acids in a protein according to their water solubility. Consequently, the presence of antibodies directly on the nanodevice surface by direct adsorption notably enhances the absorption of water molecules, resulting in increased water accumulation in close proximity to the nanodevice channel, thus more significantly affecting the electrical response.

The introduction of oppositely charged substances leads to a masking effect for the already present voltage gap and thus the antigen uptake leads to an opposite contribution to the effect introduced by the antibodies during bio-functionalization resulting in a decreased voltage gap with respect to increasing antigen concentration uptake on the sensor surface (Fig. 3, inset). Taking into consideration the abovementioned arguments, overall, it is demonstrated that the direct adsorption bio-functionalization strategy results in larger voltage gap values under high environmental humidity conditions with respect to the other two methods applied. The direct adsorption bio-functionalization method assures the largest voltage gap at 70% rH% values, presenting twice the efficiency compared to the other two methods applied for memristive bio-detection. Following these findings, it can also be concluded that a direct adsorption bio-functionalization strategy is more suitable for applications with target cancer markers at high environmental humidity values and therefore opens the possibility to provide under these environmental conditions successful sensing output using the memristive detection methodology even for lower concentrations of reagents than achievable *via* the other surface modification methodologies, highlighting the economy of reagents required for miniaturized bio-assays.

Surface and morphological analysis

Morphological analysis data obtained from AFM on the bare nanowire structures as well as the nanowire structures after bio-modification with the anti-PSA antibody are shown in Fig. 4 in order to demonstrate the attachment of the biomolecules on the nanowire structure. The AFM analysis is first performed for bare nanofabricated structures and then immediately after the bio-modification process. In Fig. 4a a Si nanowire structure anchored between two NiSi terminals after nanofabrication is depicted. In Fig. 4b the nanowire structure after bio-modification is presented. It is shown that in the case of a bare nanodevice (Fig. 4a), the shape of the nanowire is clearly distinct. After bio-functionalization a clear change in the morphology can be seen in Fig. 4b and agglomeration of biomolecules can be observed on the devices' surface. It is important to note that the nanofabricated devices are not subjected to any other intermediate step or treatment than with the biological molecules, leading to the heuristic conclusion that the morphology of the device surface is clearly changed due to the presence of biological substances. From these results, it thus becomes possible to postulate on the structural nature of the nano-systems and the tendency of the biological molecules to

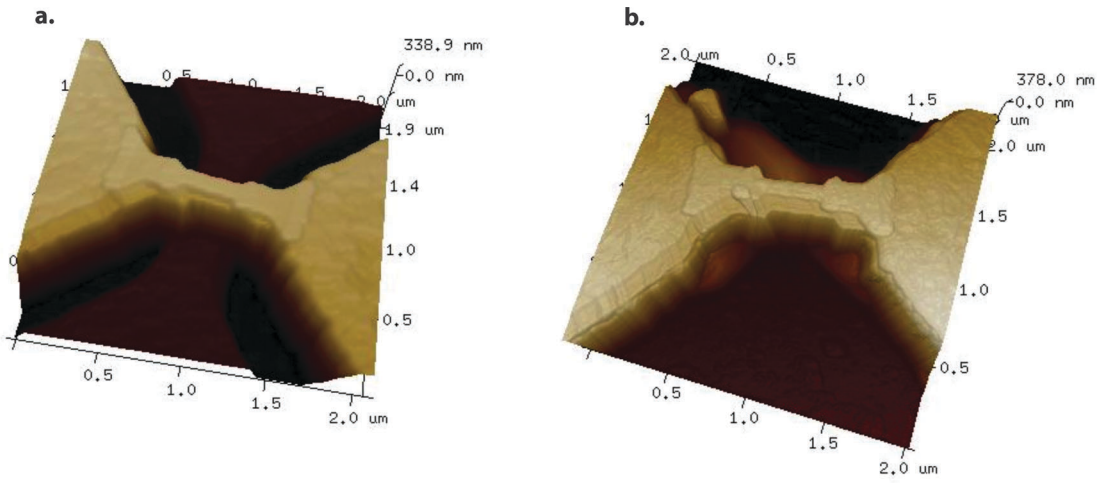

Fig. 4 AFM morphological analysis of nanofabricated structures before (a) and after the bio-modification with an anti-Prostate Specific Antigen antibody (b).

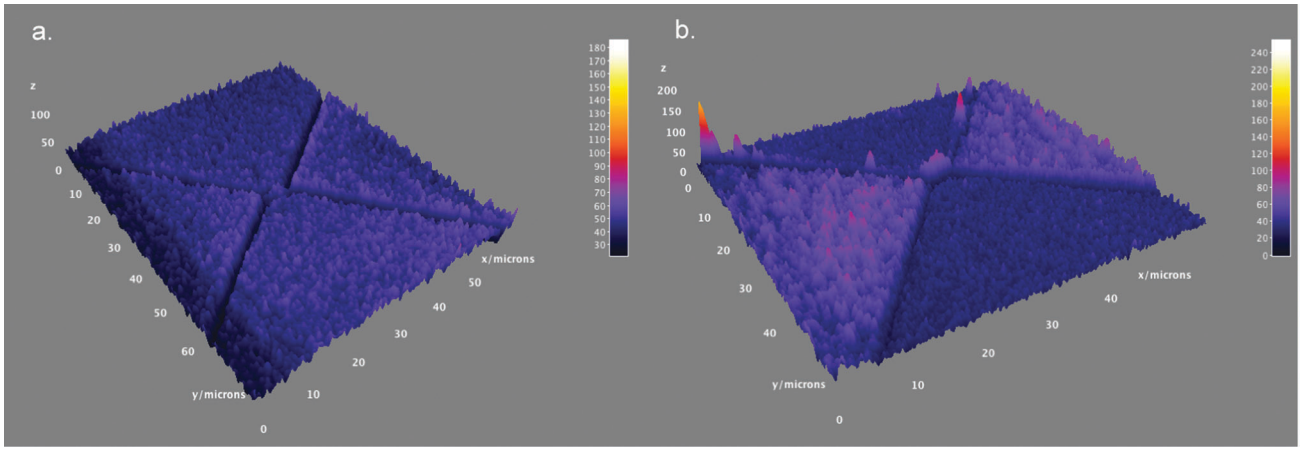

Fig. 5 3D fluorescence signal distribution acquired using CLSM from the nanofabricated structure before – control sample – (a) and after the bio-modification with FITC-conjugated antibodies (b) in the region of interest. The bright regions in the right image correspond to the accumulated biomolecule in the sample.

coalesce at the surface forming agglomerating patterns that can be observed on the structure surface.

To verify the efficiency of the binding of biomolecules on the surface of the nanofabricated structures under study 3D fluorescent signal distribution of biomolecules is obtained. The negative control sample (Fig. 5a) presents no fluorescent signal. On the other hand, Fig. 5b clearly shows the florescence emitted by the antibody-coated layer deposited onto the device surface, verifying the presence of the biomolecules. A sharp rise in the intensity of the 3D fluorescent signal is depicted in the nanostructure region with respect to the neighbouring areas of the electrodes and substrates. A further accumulation of the incubated biomolecules is also noticed in some regions, mainly at the structures' edges, which could be attributed to the equilibrium between the hydrostatics and hydrodynamics of the biological solution and the solid structure. Overall, these findings provide a further confirmation of the presence of the proteins on the sensor and the efficiency of the nanowire structures to promote bio-molecule binding.

In addition, SEM analysis of nanofabricated structures with a mean width of 90 nm and a length of 980 nm is shown in Fig. 6 after the fabrication process as well as after the bio-functionalization with the three different methodologies under study. Due to the DRIE process, the width along the structures is not perfectly homogenous, which however is an advantage for the bio-functionalization process, which promotes the increased adsorption of antibody molecules throughout the surface. In fact, the surface roughness enhances the binding of the proteins on the device by increasing the potential freely-available binding area and overall enables the bio-functionalization process. The nanostructures before and after the bio-modification process show a difference in the mean width, which suggests the presence of deposited molecules. More specifically, an increase in the mean width of the device is demonstrated due to the presence of the adsorbed layer of biomolecules on the nanowire surface. Accumulated data considering several measurements along the structures of different devices show a mean increase of the width

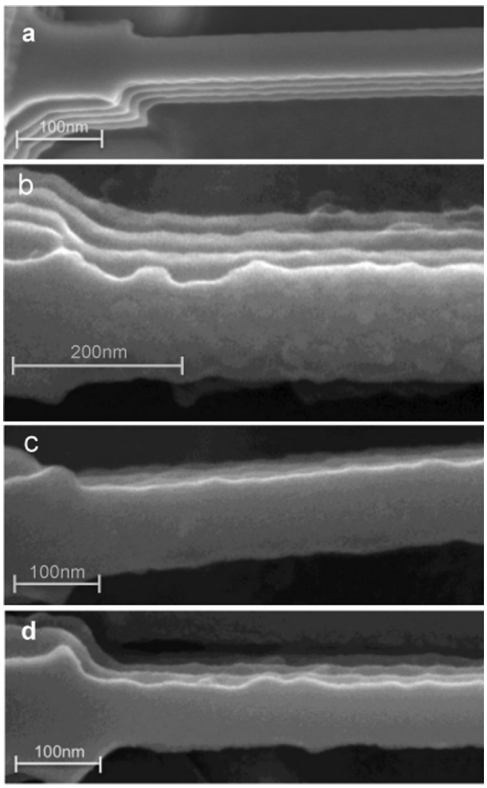

Fig. 6 SEM morphological analysis of nanofabricated structures prior to (a) and after the bio-functionalization process for nanowires of initial mean width 90 nm and 980 nm of length *via* the implementation of three bio-modification techniques; (b) affinity method, (c) covalent linkage with GPTES and (d) direct adsorption.

of the devices of 15.7 nm ± 3.1 nm for the direct adsorption bio-functionalization methodology, which is compatible with a single layer of antibodies with an expected size of approximately 14 nm (14.5 nm × 8.5 nm × 4.0 nm).[42,43] In some cases, a more significant increase of the structures' mean width reaching values

of 45.43 nm ± 3.61 nm is observed, which can be attributed to protein aggregation in these regions. Data obtained for different devices on the same substrate indicate that large agglomerations of biomolecules are quite frequently noticed on the surface as well as at the sidewalls of the devices for the direct adsorption method. Issues such as protein aggregation may also explain the deviation from ideal monolayer coating on the nanowire surface. Meanwhile, the implementation of the affinity method results in an increase in the mean width of 22.1 nm ± 4.3 nm. Considering that it is possible to model the biotin and streptavidin molecules as spheres, the thickness of a biotin layer is estimated at 1 nm and that of a streptavidin layer at 5 nm. As before, protein clustering appears, contributing to the deviation from the case of an ideal monolayer on the nanowire surface of all the bio-layers involved, namely biotin, streptavidin and antibodies. In the case of the bio-functionalization methodology using GPTES for covalent attachment, a mean increase of the device width of 17.1 nm ± 3.1 nm is measured. The theoretical thickness of a GPTES film from the Si(100) surface to the top of a molecule is calculated to be 1.3 nm using DFT calculations,[44] which also agrees with the difference of 1.4 nm noticed comparing to the value obtained from the direct adsorption measurements in this study. It is important to mention that the final GPTES-layer size is generally expected to be larger than that of a monolayer since the method used in the present study involves the incubation of the entire substrate in the reagent solution instead of chemical vapor silylation or spin-on application under dry conditions, methods that favor monolayer deposition. From the results shown, it is interesting to note the possibility to tune the degree of adsorption of molecules depending on which strategy is chosen and for which application the assay will be used.

Conclusions

In the present work, nanofabricated memristive devices are bio-functionalized through three bio-functionalization strategies, in order to design and develop optimum memristive biosensors for future applications targeting antigen sensing in general and PSA detection in particular. AFM, SEM and Confocal microscopy verify the successful uptake of the biological molecules on the device surface. The impact of the rH% and of the bio-functionalization strategy applied on the memristive signals are studied for both systems of memristive devices and memristive biosensors.

The results obtained by the electrical characterization for the bio-functionalization strategies under study indicate that all three types of the realized memristive biosensors are suitable for the specific memristive sensing mechanism. Considering that an optimum memristive biosensor should provide a starting gap as large as possible and taking into consideration the environmental humidity conditions, an optimum memristive biosensor can be defined. It is found that a direct adsorption bio-functionalization strategy demonstrates twice the efficiency with respect to the other two methods at 70% rH% values, thus will be more suitable for applications with target biomarkers under high environmental humidity conditions offering also the potential for a successful sensing output even at lower concentrations of reagents, therefore contributing to the economy required for miniaturized bio-assays.

The present study paves the way for future applications of optimized immuno-sensors for diagnostics and the implementation of the optimum memristive biosensor for successful and optimized sensing outputs with the memristive bio-detection mechanism. Furthermore, these optimized bio-functionalizations show high potential for use in memristive biosensors for LoC (lab-on-a-chip) and PoC (point-of-care) applications with appropriate integration and multiplexing aspects.

Acknowledgements

The authors gratefully acknowledge the staff of the CMI Clean Room of EPFL and M. Zervas for technical advice and fruitful discussions regarding the nanofabrication process, R. R. G. Soares for stimulating discussions regarding the bio-functionalization protocols and G. Knott for SEM imaging using a ZEISS Gemini500. The authors acknowledge financial support from the European Commission FP7 Programme through the Marie Curie Initial Training Network 'PROSENSE' (Grant No. 317420, 2012–2016). N. M. acknowledges for his post-doctoral funding from FCT grant SFRH/BPD/105402/2014.

References

1 A. Parracino, M. T. Neves-Petersen, A. Kold di Gennaro, K. Pettersson, T. Lövgren and S. B. Petersen, Arraying prostate specific antigen PSA and Fab anti-PSA using light-assisted molecular immobilization technology, *Protein Sci.*, 2010, **19**(9), 1751–1759.
2 X. L. Sun, C. L. Stabler, C. S. Cazalis and E. L. Chaikof, Carbohydrate and Protein Immobilization onto Solid Surfaces by Sequential Diels–Alder and Azide–Alkyne Cycloadditions, *Bioconjugate Chem.*, 2006, **17**(1), 52–57.
3 R. A. Vijayendran and D. E. Leckband, A Quantitative Assessment of Heterogeneity for Surface-Immobilized Proteins, *Anal. Chem.*, 2001, **73**(3), 471–480.
4 B. M. Kihlberg, U. Sjobring, W. Kastern and L. Bjorck, Protein LG: a hybrid molecule with unique immunoglobulin binding properties, *J. Biol. Chem.*, 1992, **267**(35), 25583–25588.
5 J. E. Koehne, H. Chen, A. M. Cassell, Q. Ye, J. Han, M. Meyyappan and J. Lia, Miniaturized Multiplex Label-Free Electronic Chip for Rapid Nucleic Acid Analysis Based on Carbon Nanotube Nanoelectrode Arrays, *Clin. Chem.*, 2004, **50**(10), 1886–1893.
6 F. Patolsky, G. Zheng and C. M. Lieber, Fabrication of Si nanowire devices for ultrasensitive, label-free, real-time detection of biological and chemical species, *Nat. Protoc.*, 2006, **1**(4), 1711–1724.

7 X. T. Zhou, J. Q. Hu, C. P. Li, D. D. D. Ma and S. T. Lee, Si nanowires as chemical sensor, *Chem. Phys. Lett.*, 2003, **369**(1-2), 220–224.
8 J. L. Arlett, E. B. Myers and M. L. Roukes, Comparative advantages of mechanical biosensors, *Nat. Nanotechnol.*, 2011, **6**, 203–215.
9 F. Patolsky and C. Lieber, Nanowire nanosensors, *Mater. Today*, 2005, **8**(4), 20–28.
10 G. Zheng, F. Patolsky, Y. Cuil, W. Wang and C. Lieber, Multiplexed electrical detection of cancer markers with nanowire sensor arrays, *Nat. Biotechnol.*, 2005, **23**(3), 1294–1301.
11 E. Stern, A. Vacic and A. R. Mark, Semiconducting nanowire field-effect transistor biomolecular sensors, *IEEE Trans. Electron Devices*, 2008, **55**(11), 3119–3130.
12 X. Duan, Y. Li, N. K. Rajan, D. A. Routenberg, Y. Modis and M. A. Reed, Quantification of the affinities and kinetics of protein interactions using Si nanowire biosensors, *Nat. Nanotechnol.*, 2012, **7**, 401–407.
13 M. Curreli, Z. Rui, F. N. Ishikawa, H. K. Chang, R. J. Cote, Z. Chongwu and M. E. Thompson, Real-time, label-free detection of biological entities using nanowire-based FETs, *IEEE Trans. Nanotechnol.*, 2008, **7**(6), 651–667.
14 W. N. Frost, V. F. Castellucci, R. D. Hawkins and E. R. Kandel, Monosynaptic connections made by the sensory neurons of the gill- and siphon-withdrawal reflex in Aplysia participate in the storage of long-term memory for sensitization, *Proc. Natl. Acad. Sci. U. S. A.*, 1985, **82**(23), 8266–8269.
15 A. Lendlein and S. Kelch, Shape-memory polymers, *Angew. Chem.*, 2002, **41**(12), 2034–2057.
16 J.-M. Lehn, From supramolecular chemistry towards constitutional dynamic chemistry and adaptive chemistry, *Chem. Soc. Rev.*, 2007, **36**(2), 151–160.
17 J. Wua and R. McCreery, Solid-State Electrochemistry in Molecule/TiO_2 Molecular Heterojunctions as the Basis of the TiO_2 Memristor, *J. Electrochem. Soc.*, 2009, **156**(1), 29–37.
18 L. Chua, Memristor – the missing circuit element, *IEEE Trans. Circuit Theory*, 1971, **18**(5), 507–519.
19 L. Chua and S. M. Kang, Memristive devices and systems, *Proc. IEEE*, 1977, **65**(6), 915–929.
20 D. Strukov, G. Snider, D. Stewart and S. Williams, The missing memristor found, *Nature*, 2008, **453**, 80–83.
21 Y. V. Pershin and M. Di Ventra, Memory effects in complex materials and nanoscale systems, *Adv. Phys.*, 2011, **60**, 145–227.
22 M. Haykel Ben Jamaa, S. Carrara, J. Georgiou, N. Archontas and G. De Micheli, Fabrication of Memristors with Poly-Crystalline Si Nanowires, Proceedings of the 9th IEEE Conference on Nanotechnology, 2009, pp. 152–154.
23 D. Sacchetto, M. H. Ben-Jamaa, S. Carrara, G. De Micheli and Y. Leblebici, Memristive Devices Fabricated with Si Nanowire Schottky Barrier Transistors, Proceedings of IEEE International Symposium on Circuits and Systems (ISCAS), 2010, pp. 9–12.
24 D. B. Strukov, D. R. Stewart, J. Borghetti, X. Li, M. Pickett, G. M. Ribeiro, W. Robinett, G. Snider, J. P. Strachan, W. Wu, Q. Xia, J. J. Yang and R. S. Williams, Hybrid CMOS/Memristor Circuits, Proceedings of 2010 IEEE International Symposium on Circuits and Systems, 2010, pp. 1967–1970.
25 T. Berzina, A. Smerieri, M. Bernabo, A. Pucci, G. Ruggeri, V. Erokhin and M. P. Fontana, Optimization of an organic memristor as an adaptive memory element, *J. Appl. Phys.*, 2009, **105**, 124515.
26 T. W. K. Dong Ick Son, J. H. Shim, J. H. Jung, D. U. Lee, J. M. Lee, W. I. Park and W. K. Choi, Flexible organic bistable devices based on graphene embedded in an insulating poly(methyl methacrylate) polymer layer, *Nano Lett.*, 2010, **10**(7), 2441–2447.
27 E. Lehtonen and M. Laiho, CNN using memristors for neighborhood connections, Proceedings of 12th International Workshop on Cellular Nanoscale Networks and Their Applications (CNNA), 2010, pp. 1–4.
28 D. Sacchetto, G. De Micheli and Y. Leblebici, Multi-terminal Memristive Nanowire Devices for Logic and Memory Applications: A Review, *Proc. IEEE*, 2012, **100**(6), 2008–2020.
29 S. H. Jo, T. Chang, I. Ebong, B. B. Bhadviya, P. Mazumder and W. Lu, Nanoscale memristor device as synapse in neuromorphic systems, *Nano Lett.*, 2010, **10**(4), 1297–1301.
30 G. Rose, J. Rajendran, H. Manem, R. Karri and R. Pino, Leveraging Memristive Systems in the Construction of Digital Logic Circuits, *Proc. IEEE*, 2012, **100**(6), 2033–2049.
31 Y. Pershin and M. Di Ventra, Experimental demonstration of associative memory with memristive neural networks, *Neural Networks*, 2010, **23**(7), 881–886.
32 G. Indiveri, B. Linares-Barranco, R. Legenstein, G. Deligeorgis and T. Prodromakis, Integration of nanoscale memristor synapses in neuromorphic computing architectures, *Nanotechnology*, 2013, **24**, 384010.
33 A. Gelencser, T. Prodromakis, C. Toumazou and T. Roska, Biomimetic model of the outer plexiform layer by incorporating memristive devices, *Phys. Rev. E: Stat., Nonlinear, Soft Matter Phys.*, 2012, **85**, 041918.
34 D. Sacchetto, P. E. Gaillardon, M. Zervas, S. Carrara, G. De Micheli and Y. Leblebici, Applications of Multi-Terminal Memristive Devices: A Review, *IEEE Circuits Syst.*, 2013, **13**(2), 23–41.
35 P. E. Gaillardon, D. Sacchetto, S. Bobba and Y. Leblebici, GMS: Generic Memristive Structure for Non-Volatile FPGAs, IEEE/IFIP 20th International Conference on VLSI and System-on-Chip (VLSI-SoC), 2012, pp. 94–98.
36 D. Sacchetto, M. A. Doucey, G. De Micheli, Y. Leblebici and S. Carrara, New Insight on Biosensing by Nano-fabricated Memristors, *BioNanoScience*, 2011, **1**, 1–3.
37 S. Carrara, D. Sacchetto, M. A. Doucey, C. Baj-Rossi, G. De Micheli and Y. Leblebici, Memristive-biosensors: a new detection method by using nanofabricated memristors, *Sens. Actuators, B*, 2012, **171–172**, 449–457.
38 I. Tzouvadaki, F. Puppo, M.-A. Doucey, G. De Micheli and S. Carrara, Computational Study on the Electrical Behavior

of Silicon Nanowire Memristive Biosensors, *IEEE Sens. J.*, 2015, **15**(11), 6208–6217.

39 D. D. Eley, in *Semiconductivity in Biological Molecules*, Horizons in Biochemistry, ed. M. Kasha and B. Pullman, Academic press, New York, 1962, pp. 341–380.

40 D. D. Eley, Semiconducting Biological Polymers, in *Organic Semiconducting Polymers*, ed. J. E. Katon, Detter, New York, 1968, pp. 259–294.

41 P. R. Gascoyne, R. Pethig and A. Szent-Gyorgyi, Water structure-dependent charge transport in proteins, *Proc. Natl. Acad. Sci. U. S. A.*, 1981, **78**(1), 261–265.

42 T. C. Werner, J. R. Bunting and R. E. Cathou, The Shape of Immunoglobulin G Molecules in Solution, *Proc. Natl. Acad. Sci. U. S. A.*, 1972, **69**(4), 795–799.

43 Y. Horng, T. M. Liu, B. Nolting, J. G. Go, J. Gervay-Hague and G. Y. Liu, A Nanoengineering Approach for Investigation and Regulation of Protein Immobilization, *ACS Nano*, 2008, **2**(11), 2374–2384.

44 G. B. Demirel, N. Dilsiz, M. Çakmakc and T. Çaykaraa, Molecular design of photo switchable surfaces with controllable wettability, *J. Mater. Chem.*, 2011, **21**, 3189–3196.

